Morphological Variations of Explosive Residue Particles and Implications for Understanding Detonation Mechanisms.

Nadia Abdul-Karim,*[§] Christopher S. Blackman,[§] Philip P. Gill,[¥] Ruth M. Morgan,[‡] Lidija Matjacic,[±] Roger Webb[±] and Wing H. Ng.[ϕ]

[§] Christopher Ingold Laboratories, Department of Chemistry, University College London, 20 Gordon Street, London, WC1H 0AJ, UK. nadia.abdul-karim.10@ucl.ac.uk

[¥] Centre for Defence Chemistry, Cranfield University, Defence Academy of the United Kingdom, Shrivenham, SN6 8LA, UK.

[‡] Centre for the Forensic Sciences, Department of Security and Crime Science, University College London, 35 Tavistock Square, London, WC1H 9EZ, UK.

[±] Surrey Ion Beam Centre, Nodus Laboratory, University of Surrey, Guildford, Surrey, GU2 7XH, UK.

[ϕ] Department of Electronic and Electrical Engineering, Faculty of Engineering Sciences, University College London, Torrington Place, WC1E 7JE, UK.

ABSTRACT: The possibility of recovering undetonated explosive residues following detonation events is well known, however, the morphology and chemical identity of these condensed phase post-blast particles remains undetermined. An understanding of the post-blast explosive particle morphology would provide vital information during forensic examinations, allowing rapid initial indication of the explosive material to be microscopically determined prior to any chemical analyses, and thereby saving time and resources at the crucial stage of an investigation. In this study, condensed phase particles collected from around the detonations of aluminized ammonium nitrate and RDX-based explosive charges were collected in a novel manner utilising SEM stubs. By incorporating the use of a focused ion beam during analysis, for the first time it has been possible to determined that such particles have characteristic shapes, sizes and internal structures depending on the explosive and the distance from the detonation at which particles are recovered. Spheroidal particles (10 µm to 210 µm) with micro surface features recovered following inorganic charge detonations were dissimilar to the irregularly shaped particles (5 µm to 100 µm) recovered following organic charge firings. Confirmatory analysis to conclude the particles were indeed explosive included HPLC-MS, Raman spectroscopy and MeV-SIMS. The results impact not only on forensic investigation but also on the theoretical constructs which govern detonation theory by indicating the potential mechanisms by which these particles survive and how this varies between the different explosive types.

Introduction

The use of explosive devices by criminals and terrorist groups poses a significant threat around the world, endangering public safety as well as causing political and economic instabilities. Preventing the illegal use of explosives is clearly paramount in counteracting such negative impacts, however as demonstrated through high profile incidents around the world, such as bombings in Bangkok, Boston, London, and Mumbai, this is not always possible. Following explosion attacks, investigative efforts focus on the crime scene and aim to answer questions regarding the nature of the event using forensic evidence.[1] Primarily, the recovery and analysis of trace chemical evidence can determine the explosive used, and thereby provide intelligence that enables crime reconstruction and identify perpetrators.[2]

Post-blast explosive residues remaining after an explosion are more readily identifiable following incomplete or partial detonations (due to some failure in the detonator for example), appearing as 'chunks' of explosive. Even in the case of apparently complete detonations, trace undetonated explosive residue particles can still be recovered. [3, 4] The mechanism by which these residues persist during high-order detonations is unknown [4] and yet it is these chemical traces which provide the diagnostic information required to indicate whether the explosive was home-made, commercial, military or associated with a particular terrorist organization. Upon collection of debris items at the scene, microscopic examinations establish the presence of particulate matter, which if apparent is swabbed and analyzed with confirmatory techniques. [5] Given that initial assessments can often involve microscopy, knowledge of the morphological characteristics of post-blast residues of an explosive would be valuable in rapidly determining the explosive type, yet few attempts have been made to do so.

Published work has focused predominantly on establishing the physical and chemical characteristics of post-blast pyrotechnic residues, [6-9] which have been found to consist of spherical particles with diameters of either less than 1 µm, [6] or between 5 µm and 20 µm. [7, 8] In most cases the elemental compositions of the observed particles, obtained using scanning electron microscopy – energy dispersive x-ray spectroscopy (SEM-EDS), were consistent with the 'pre-blast' pyrotechnic material (e.g. containing Al, Mg, Cl, K, St, Ba, etc.). [9] Corresponding knowledge for high explosive post-blast particles is limited to studies which have investigated the residue remaining following firings of Composition B (an explosive composition containing trinitrotoluene (TNT) and trimethylenetrinitramine (RDX)); the post-blast residues were found to consist of individual spherical particles [10] and quasi-spherical particles coalesced and joined as aggregates. [11] In either case however, no findings regarding any other morphological distinctions between the TNT or RDX particles were provided. With regard to the size of post-blast explosive particles, a recent study [12] found the majority to range between 10 µm and 30 µm in diameter, however details of the explosive materials that were fired and any variations in the particle sizes based on explosive charge types were not discussed.

Despite the paucity of experimental information regarding the process by which explosive residue particles can remain undecomposed during detonations, it is expected that their physical morphology would vary from that of the particles prior to detonation. The high temperatures (> 5000 K) and pressures (up to 100 GPa) [3] in the reaction zone of the explosive would cause defects in the original explosive crystals at the very least. If particles were ejected from the bulk of the explosive (from the charge surface for example) it is plausible that they may vaporize or melt and move as molten airborne material, solidifying during dispersion due to localized decreases in temperature. [7, 8] Due to drag effects on molten matter rapidly moving through air, the resulting particles, once condensed, could appear spherical. It is unknown whether this mechanism would apply for all types of explosives and it could be considered that variations in the reaction chemistry of different energetic materials would manifest in the morphology of post-blast particles of each.

In this work, we investigate the morphological variations between the post-blast particles of two different explosive formulations, aluminized ammonium nitrate (AlAN), an improvised explosive mixture, and Plastic Explosive No. 4 (PE4) (which is an RDX–based military composition). We use novel, simple methods to capture the post-blast particles and our morphological analysis comprises of imaging with SEM as well as using a less conventional explosive analysis tool, a focused ion beam, to probe the internal structure of the residues. Finally, the chemical identity of the particles as explosive residues is established using Raman spectroscopy, ion chromatography (IC), high performance-liquid chromatography (HPLC-MS) and mega-electron volt–secondary ionisation mass spectrometry (MeV-SIMS) methods.

Experimental section

Materials

Explosives and all precursor materials were provided by the UK Defence Academy. The AlAN and PE4 explosives were moulded into spherical 0.5 kg charges and electrically initiated to produce detonation. Prior to initiation, each detonator was positioned vertically, into the middle of the charge, with the detonator tip facing towards the top of the charge. All charges were initiated this way in order to avoid directionally biased expansion of the product gases from any of the firings and thereby attempt to maintain consistency between detonations.

Methods

Explosive charges were positioned on top of firing poles, 2 m from the ground on the central firing areas of the explosive range at Cranfield University. Post-blast particulate material was directly captured onto the surfaces of aluminium SEM specimen stubs (12.5 mm diameter and 3.20 mm diameter pin with groove; Taab Laboratories, UK), each coated with a double sided adhesive carbon tape disc. Using adhesive, the SEM stubs were attached on an array of sampling poles that were positioned at 1 m incremental distances from the central firing pole in four orientations about the centre, and up to 10 m away from it (Figure 1a and b). The poles were not positioned in tandem with each other in order to avoid obstruction of the furthest positioned SEM stubs from those closer to the detonation centre. Each formulation type was fired 6 times; Figure 1c shows the blast-wave visible around the fireball of a typical PE4 detonation, captured with a Phantom V12.1 high-speed imaging camera (6000 frames per second). Following each firing, the base of each stub was removed from the adhesive mounts with tweezers and placed within a labelled single SEM pin stub storage tube (25 mm diameter, 55 mm height; Taab Laboratories, UK) (Figure 1d). Care was taken not to touch the stub surface during the procedure.

Figure 1. Schematics of sampling pole layout and stub arrangement around detonations: a) placement of SEM stubs onto steel sampling poles using adhesive mounts, b) aerial view of the sampling poles (black) positioned at 1 m incremental distances around the central explosive charge, c) example of fireball during detonation of PE4 charge, and d) individual sample holders used to store collected stubs following each firing.

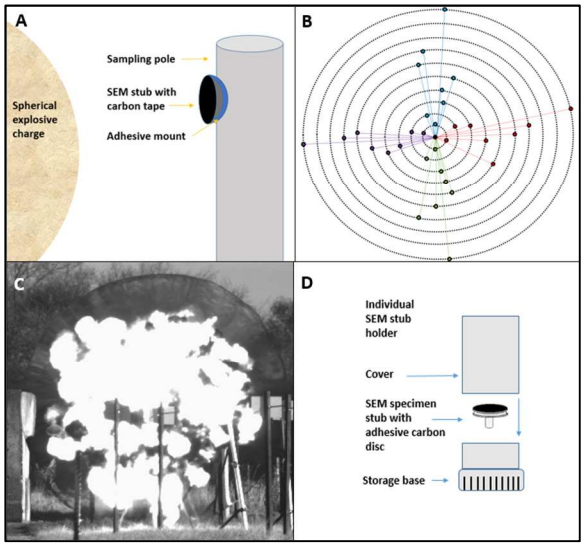

Analytical

Scanning Electron Microscopy-Energy Dispersive X-ray Spectroscopy (SEM-EDS) analysis was performed with a Hitachi S-3400N variable pressure system, which allowed the study of the uncoated, non-conductive samples. Imaging was conducted in secondary electron imaging mode. Beam current = 10 nA; spot size = 30 µm; chamber pressure = 20 Pa to 30 Pa (air); working distance = 10 mm; accelerating potential voltage = 5 kV to 15 kV.

Raman spectroscopy was conducted using a Renishaw InVia Raman microscope (785 nm NIR laser; 0.1 % to 10 % intensity), with 5 accumulations collected over 10 – 15 second exposures).

Focused Ion Beam-SEM (FIB-SEM): Samples were sputtered with Au for 30 seconds prior to analysis. The milling of particles was performed in a focused ion beam system (Zeiss XB1540 CrossBeam FIB). Gallium ions were used for the milling process. The beam current used for the initial milling was typically 1 to 2 nA. The surface of the milled particles was polished and it was carried out at a much lower beam current, typically 100 to 200 pA. The images of the particles before and after the milling were taken by the same system with a built-in thermal field emission SEM. Typical SEM operating conditions: resolution = 1.1 nm at 20 kV, 2.5 nm at 1 kV, accelerating voltage = 0.1 kV to 30 kV. Typical FIB operating conditions: resolution = 7 nm at 30 kV, accelerating voltage = 3 kV to 30 kV, emitter = Ga liquid metal ion source.

MeV-SIMS measurements were collected using a 2 MV Tandetron (High Voltage Engineering, Europe) at the Surrey Ion Beam Centre. An 8.8 MeV O^{4+} beam focused to 4 µm resolution was used as a primary ion. A quadrupole triplet lens system (Oxford Microbeams Ltd.) focused the beam and allowed electrostatic scanning over an area of 2 mm^2. The MeV ion beam exited the vacuum system through a Si_3N_4 window (100 nm thick). Secondary ions were carried through the capillary (50 cm length, 700 mm and 2 mm distance from spot size) using helium flow into Q-TOF orthogonal mass spectrometer (detection interval between *m/z* 50 and *m/z* 1000). The working current was <50 pA and spectra were collected for 5 min.

Ion Chromatography analysis was perfomed on a Dionex ICS-2000 reagent free IC system with eluent generation (Thermo Scientific, USA) coupled to an SRS-300 autosuppression device and conductivity detector. Collected particles were solubilized in 5 cm^3 of deionised water (18 MΩ) and the solutions filtered through 0.2 µm pore nylon prior to injection. Operating conditions for anion (NO_3^-) and cation (NH_4^+) analyses were: column = IonPac AS19 4.0 mm x 250 mm / IonPac CS16 5 mm x 250 mm, mobile phase = isochratic 22 mM KOH / isochratic 30 mM MSA, flow rate = 1 ml/min, injection volume = 100 µl, cell heater = 35°C / 40°C, pump (backpressure) = 2300 psi, detector = ECD suppressed conductivity, suppressor type = ASRS (4 mm) at 112 mA / CSRS-ULTRA (4 mm) at 100 mA, sample run time = 20 mins/30mins. In order to quantify the ions in the post-blast samples, ten series calibration standards (1 µg/L to 1000 µg/L) of nitrate and ammonium were prepared in deionised water.

High Performance Liquid Chromatography (HPLC) separation was performed with a Dionex UltiMate 3000 single capillary LC system using an Acquity BEH C-18 column (2.1 mm x 50 mm, 1.7 µm particles, 130 Å). Collected particles were solubilized from the stubs in 5 cm^3 of acetone, which was filtered and evaporated; the remaining residue was re-solubilized in acetonitrile prior to analysis. The mobile phases were 0.1 % $CHCl_3$ in DI water (mobile phase A) and 0.1 % $CHCl_3$ in acetonitrile (mobile phase B); the flow rate was 200 µl/min. The total sample run time was 10 minutes. Samples were held in an auto-sampler tray kept at 4 °C and 10 µl injections were loaded onto the column via a partial sample loop mechanism. Between sample injections, the injector and needle were flushed and washed with methanol to minimise carry-over of RDX between injections. Blank acetone and acetonitrile samples were also run throughout the sample sequence to ensure minimal carry over. In order to quantify the RDX in the post-blast samples, ten series calibration standards (1 µg/L to 1000 µg/L) of RDX were prepared in acetonitrile.

Mass Spectrometry (MS) analyses were performed on an LTQ Ion Trap MS instrument fitted with an electrospray ionisation (ESI) source. In order to produce adducts amenable to ESI, all test and reference samples of RDX were spiked with 0.1 % $CHCl_3$ in order to form $[M+^{35}Cl]^-$ and $[M+^{37}Cl]^-$ adducts. Selected ion monitoring mode (negative) was used for the *m/z* 257 and *m/z* 259 (corresponding to the $[M+^{35}Cl]^-$ and $[M+^{37}Cl]^-$) precursor ions. Conditions were: ESI spray voltage = 5.00 kv; spray current = 30 µA; capillary temperature = 275 °C; sheath gas flow rate = 30; auxiliary gas flow rate = 10; collision energy = 35; isolation widths = 2; scan number = 5 averaged micro-scans; injection time = 200 ms.

Results and Discussion

With the use of standard techniques (e.g. SEM and chromatography) coupled with the application of non-conventional explosive analysis methods (e.g. focused ion beam analysis), we have found unique post-blast particles are produced from AlAN and PE4 charges. This finding is not only novel, but alludes to the mechanism by which they were formed, or 'survived', detonation. The process is hypothesised to vary based upon the explosive charge type due to specific complexities of each decomposition mechanism. The different reaction rates and sizes of the reaction zones, caused by the difference between the molecular explosive (RDX) and fuel-oxidiser mixture (AlAN), as well as the potentially non-uniform temperature and pressure profiles within the subsequent fireball, produce distinctly shaped post-blast particles. These findings are the most substantial attribution to date of the confirmatory peaks produced for example by HPLC analysis, which demonstrate the presence of trace explosive residue at post-blast crime scenes.

Post-blast Aluminised Ammonium Nitrate particles

In order to produce the AlAN formulations, AN prills (Figure 2a) were ground down and mixed with flaked aluminium. The ground AN particles varied in size between 30 µm and 1300 µm in diameter (Figure 2b), and the aluminium was clearly visible upon the particle surfaces (Figure 2c and d).

The surfaces of the collected SEM stubs, particularly those positioned closest to the AlAN detonations at 1 m and 2 m, were typically heterogeneously coated with an assortment of particles, most notably sediment particles rebounded from the ground (example micrographs of which are in Figure S-1 in the SI). In order to locate material thought to be post-blast

Figure 2. SEM micrographs of a) AN prill surface, b) ground AN particles, c) AN particles once mixed with Al, d) close-up of Al flakes on AN particle surface, e–h) representative post-blast particles observed on stubs retrieved 1 m from the detonations of 0.5 kg AlAN charges, i–l) particles retrieved from 2 m and 3 m distances, m–p) particles retrieved from 4 m to 7 m distances.

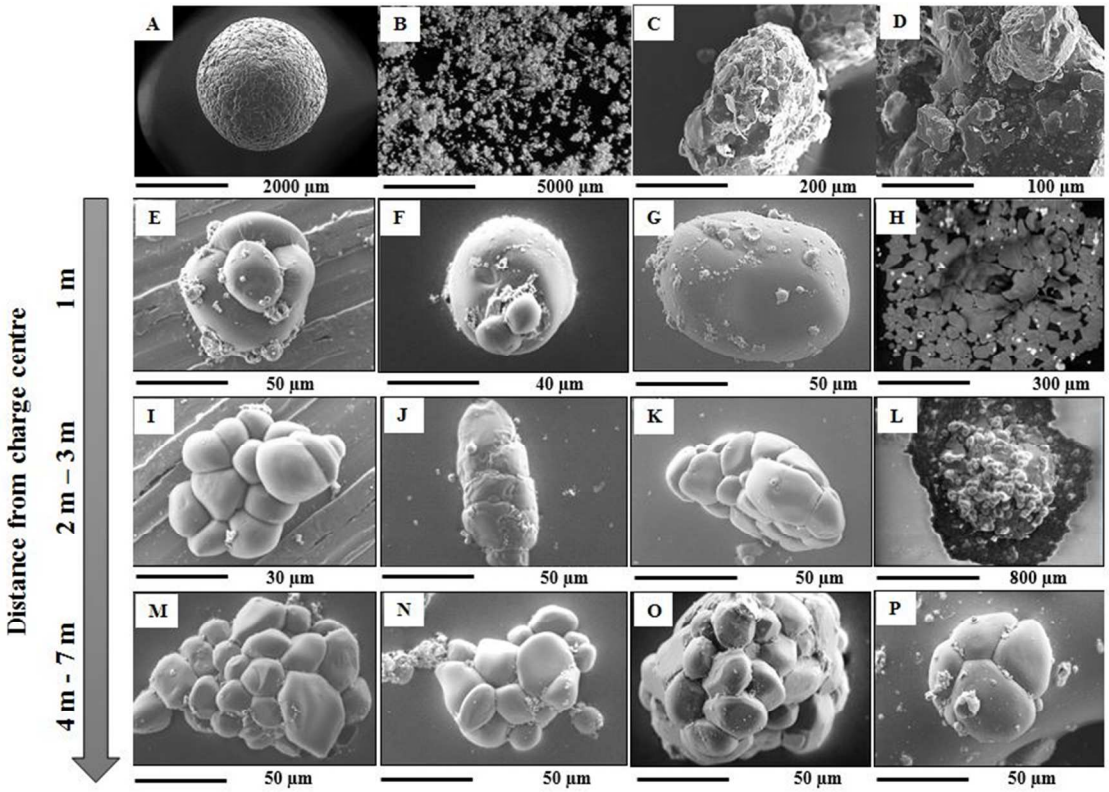

AlAN residue, SEM-EDS was used to find particles with elemental compositions consistent with that of the explosives, specifically consisting of only N, O, Al and C (the presence of carbon being ubiquitous in most particles). The atomic percentages of the elements present in the post-blast particles varied to those of the undetonated material (see Table S-1 in SI). Discrepancies were likely due to a number of reasons including the loss of more volatile components during detonation, the presence of carbon and oxygen in the adhesive tape on the stubs, and issues with the detection of 'light' elements with EDS, which is known to be limited when using a Be window detector. [13] EDS was therefore used as an effective screening tool, with Raman spectroscopy used to establish the chemical identity of particles ascribed to be post-blast explosive residues.

The observed particles were grouped into distance 'bins' of '1 m', '2 m to 3 m' and '4 m to 7 m' from the detonation, these groupings were designated through the identification of morphologically similar particles being identified within each. Figure 3 shows a representative spectrum of particles from each of these grouped distances, plotted with that of the undetonated particles, and compared to a 'blank' spectrum of the adhesive carbon disc present on the SEM stubs. In all cases, the majority of dominant bands present in the undetonated material were exhibited in the post-blast particles, confirming for the first time, their provenance being the AlAN explosives; features corresponding to the characteristic bands in Figure 3 are provided in Table S-2 in the SI. As the size of the observed particles increased with increasing distance from the detonations (Figure 2), the intensity of the Raman bands also followed the same trend, as expected. No bands from the adhesive background conflicted significantly with the regions of dominant explosive–related bands.

Figure 3. Raman spectrum of pre-blast AlAN particles (black) compared to representative spectra of post-blast particles collected at 1 m (red), 2 m to 3 m (blue), and 4 m to 7 m (pink) from the detonations. The green spectrum is of the adhesive carbon background.

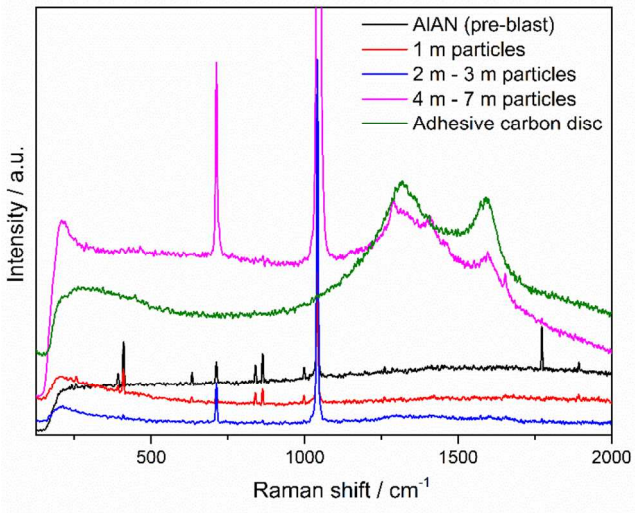

Particle sizing was established by systematically scanning each stub surface during SEM analysis, counting the number of particles and recording the diameter of each as measured with the software calipers. Statistical treatment of this data was inherently problematic given that the number of deposited particles was naturally low in the first instance and the sampling area was limited to the ~120 mm^2 per stub. The use of larger surfaces would have potentially allowed the collection of a larger number of particles, however this would not have been amenable to SEM analysis and also could have caused obstruction of sites positioned further from the firings. Additionally, while automated particle size counting analysis is possible (and more accurate than doing so manually), there is currently no viable option for automated counting of light element-based particles of non-uniform shapes. Therefore, the average particle size ranges determined per grouped distance is included herein as the most appropriate, meaningful measure for comparison, with further discussion of this topic, as well as mean averages and standard deviations of particle sizes presented in Figure S-10 and Table S-4 in Section 4 of the SI.

Evidence of residual explosive moving through the surrounding air as molten material and cooling during flight was exhibited as smooth-surfaced, spheroidal particles (72 % of particles were between 30 µm and 120 µm in diameter on average) found at the closest sampled distance of 1 m from the AlAN detonations (Figure 2e – g). The melting point of AN (~440 K) would certainly have been reached throughout the bulk of the explosive charge following initiation and it is feasible that any molten fluid formed may have been expelled away from detonation centre, [7, 8] moving ahead of the expanding product gases and thereby remaining undecomposed. Still fluid upon interaction with a sampling site, instead of particulate form, the coalescence of the molten explosive manifested as flattened, broader (> 300 µm) smeared deposits at 1 m (Figure 2h), which were the only residue form in which aluminium flecks were seen.

Where surface features were apparent on particles, they consisted of smaller (10 µm to 80 µm) fines upon the major particle surface (e.g. Figure 2f). Such smaller particles (~10 µm) were also observed independently (Figure 4) and when found in this form, often had cracked surfaces revealing hollow internal structures. The finding of hollow, cracked particles suggests that the residual explosive may have been vaporised or molten as it moved through the air, and surface tension and drag effects on the fluid would cause the exterior to harden first and upon impact onto a surrounding surface, any unsolidified fluid matter in the interior could have been ejected from the particle to leave a hollow shell structure.

The internal structure of the post-blast residues was investigated for the first time by milling the particles with a focused ion beam of Ga^+ ions that was used to sputter half of the particle (removed as either secondary ions or neutral atoms), and from which the secondary electrons produced were used to form images of the internal structure. Prior to firing, the AN particles were mainly solid and dense (Figure 5a and b). The spheroidal post-blast particles found at the 1 m distances were hollow with porous shells (Figure 5c– e), the liquid explosive may have encapsulated air pockets during flight, essentially forming bubbles of minimal surface area which cooled and solidified into such hollow spheres. [14]

Figure 4. Hollow particles and particle clusters observed on stub surfaces that were positioned 1 m from the detonations of 0.5 kg AlAN charges.

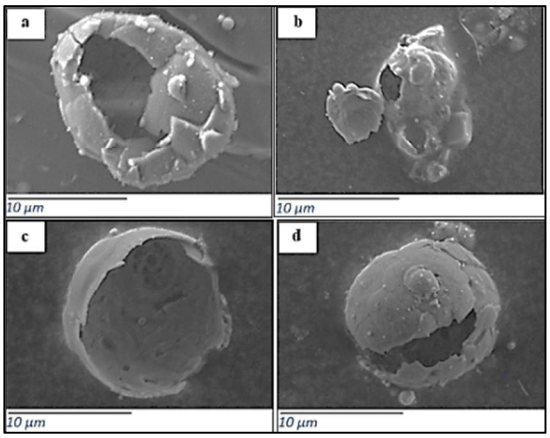

Figure 5. SEM micrographs of the internal morphology of undetonated AlAN particles (a and b). Micrographs of post-blast particles prior to being cut (c, f, i), after milling (d, g, j), and close-ups of the internal structure (e, h, k) for: spherical particles with surface features found at 1 m from detonations (c - e); smooth surfaced spheroidal particles from 2 m away (f - h); and aggregated particle clusters found 5 m away (i - k).

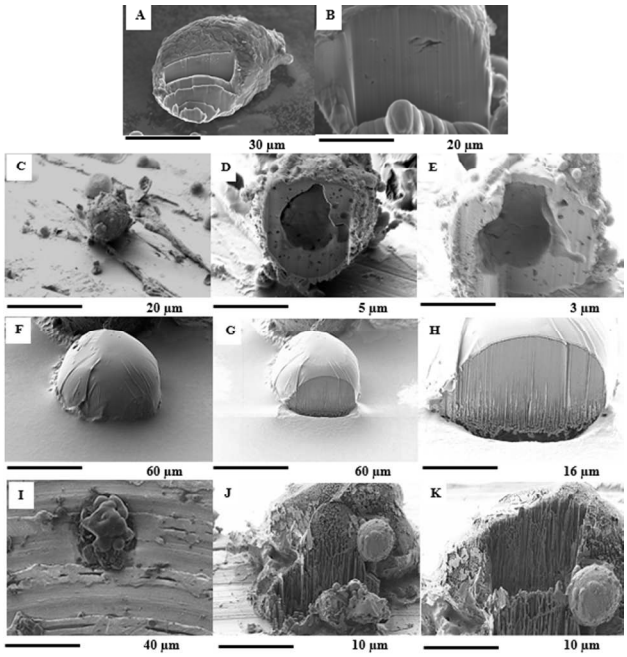

Further from the detonations, at 2 m and 3 m, the majority of post-blast AlAN residue was in the form of particle clusters (Figure 2i - k) which resembled the morphology of the undetonated whole AN prill (c.f. Figure 2a). With a particle diameter range of 30 µm to 250 µm (86 % of particles), these particles were larger overall than those observed at 1 m. Solid AN prills can be formed by spraying concentrated AN 'melt' into the top of prill towers; the molten droplets fall counter-current to a rising stream of air that cools and solidifies clustered droplets into their spherical forms. [15] The resulting prills are

therefore agglomerated particles as exhibited in their surface morphology (Figure 2a).

Had the inorganic formulations deflagrated (which pure AN is amenable to, compared to detonation), [16] the finding of post-blast particles that were morphologically similarly to their pre-blast counterparts could be explained simply by this slower-rate combustion process, which produces more residual undetonated material. However, the use of a high-explosive booster charge to produce a shock-to-detonation transition, as well as grinding of the AN prills to increase the initial burn rate, [17] and the incorporation of aluminium particles to facilitate and intensify explosion, [18] were steps taken to ensure that detonation occurred. Therefore, the finding of particles that were similar to the undetonated form suggests that additionally to the residual AlAN being formed from a fluid, particles from the bulk charge (i.e. the crushed fragments of the original AN prills) may also separate in the very early stages of detonation and remain solid. This is most likely to occur at the periphery of the explosive charge, and so it is proposed here that as the shockwave propagates through the bulk explosive, these particles are spalled from the charge surface due to local pressure rises and are ejected prior to any interaction with the shockwave or incorporation into the reaction zone where the parent molecules rapidly decompose. They may not melt as the temperature profile near the charge surfaces would be much lower than that near the initiation point and in the reaction zone. Additional support for this is that the internal structures of the undetonated AN particles (Figure 5a and b) and those post-blast particles found at 2 m and 3 m (Figure 5f – h) were similarly dense throughout rather than hollow. Larger clusters (up to 1000 µm in diameter), moving away from the bulk charge surface with greater kinetic energy, may have impacted onto the surfaces at high velocity to deposit as particle mounds surrounded by flattened surrounding edges (e.g. Figure 2l). [19]

Losing energy whilst moving further away from the detonation centre, the velocity of particles would have been lower upon impact on surfaces at 4 m to 7 m, and therefore no flat or smeared residue deposits were seen at these distances. Most residues here were in the form of larger particle aggregates; discernible individual particles ranged between 10 µm to 150 µm in diameter and the majority (42 %) of cluster diameters were ~500 µm (Figure 2m–p). The internal structures of the aggregated particle clusters were not dense within, displaying some porosity with hollow striations observed through the particles (Figure 5j and k). These were not attributed to damage from the Ga^+ beam during FIB analysis (as considered so for the striations visible in Figure 5g and h) and were thought to be a real feature due to translation of the internal structure characteristics down through the particles, although the reason for their occurrence is unknown.

No smooth-surfaced spheroidal or hollow particles were found between 4 m and 7 m, implying the trajectory of residual explosive that is molten to be shorter range than that which is spalled as solid particles from the charge surface. And no particles, of any type, were found on the stub surfaces that were positioned further than 7 m from the detonations, in any of the sampled orientations around the firings.

Whilst the number of observed particles decreased with increasing distance from the detonation, without density information, attempts to quantify the mass of explosive residue on each stub based only on particle counting was impossible. Stub surfaces were therefore washed in 5 cm^3 DI water and the amount of nitrate and ammonium quantified per surface using IC. On average, a total of approximately 400 ±187 µg was detected from the four sites positioned at 1 m, the variability of which was based on the 6 repeated firings of the charge. The amount decreased with increasing distance to 147 ± 82 µg (2 m), 92 ± 23 µg (3), 26 ± 13 µg (4) and 11 ± 9 µg (5 m). Such a trend is comparable with previous studies that have also found the amount of AN to decrease accordingly with increasing distance from a detonation. [20,21] Without being able to distinguish between ammonium/nitrate contributions from the explosive and that potentially from any deposited sediment, these quantifications are suggestive at best and cannot be associated accurately to the particle number observed on each stub (see Section 4 and Figure S-11 of the SI for more discussion of inorganic quantification).

Post-blast PE4 particles

The stable form of RDX at room temperature (α-RDX) has an orthorhombic crystal structure as seen in Figure 6a. When amassed within a plasticizer matrix to form a plastic explosive (PE) composition, discernible particles have a diameter of between approximately 10 µm to 500 µm (Figure 6b and c) and are therefore smaller than the pre-blast AlAN particles.

The post-blast particles observed after firings were grouped into distance 'bins' of '1 m', '2 m and 3 m', and '4 m and 5 m' from the detonations; these groupings were chosen as morphologically similar post-blast PE4 particles were observed within each. No particles, of any type, were seen on stubs retrieved further than 5 m from the detonations. EDS was used as a screening tool for targeting relevant particles for further analysis, and, as for similar reasons given for AlAN, whilst the elemental compositions of particles were consistent with the undetonated material, the elemental atomic percentage ratios were not (see Section 3 of the SI for data).

Attempts to analyse the post-blast PE4 particles with Raman spectroscopy were unsuccessful as identification with the microscope was inherently challenging given the presence of larger irrelevant matter on the stubs (such as sediment particles). The presence of particles containing RDX was therefore initially established with ambient pressure MeV-SIMS; this is the first application of this technique to explosives analysis. Figure 7 shows a comparison between representative MeV-SIMS spectra of undetonated and post-blast PE4 particles recovered from 2 m and 3 m distances (these were the largest particles and therefore those which could be identified). The intense peaks in both spectra at *m/z* 221.18 were consistent with the molecular mass of RDX (222.12 Da).

The main challenge of performing MeV-SIMS analysis under ambient pressure conditions is the need to overcome the background contribution in the spectra; conflicting peaks from the carbon adhesive tape were also present in the 220 to 224 *m/z* range (green spectrum in Figure 7). Polydimethylsiloxane $(C_2H_6OSi)_n$,) is a likely component of the adhesive and can fragment into molecules of ~222 Da; despite these having a much lower intensity than the signal originating from the particles, they complicate the undisputable assignment of the peaks in the spectra to being that of the explosive only.

Confirmation for the presence of RDX was subsequently established using HPLC-MS; stubs were washed in 5 cm^3 of acetone and the solutions filtered through 0.2 µm pore nylon filters before being evaporated and the residues resilubilised in acetonitrile prior to injection. The ions at *m/z* 257 and *m/z* 259 in the mass spectra were adducts of RDX and chlorine (^{35}Cl and ^{37}Cl respectively) (see section 3 of the SI for further HPLC-MS and MS/MS data). While it was not possible to assign the provenance of individual particles to the explosive, the existence of explosive matter on the stubs was determined conclusively. And with no other visible particle types observed (apart from sediment), those particles ascribed to be post-blast PE4 were thought to be the source of such signals.

The majority of post-blast PE4 residue particles at the closest sampled distance of 1 m from the detonations had smooth-edged, folded and curved shapes (66 % of which were 10 µm to 100 µm in diameter, Figure 6d–g); none resembled their undetonated form. The formation mechanism for such particles is currently unknown. Computational efforts have determined distinct temporal stages during the decomposition of RDX, which include the rapid production of N_2 and H_2O within picoseconds, followed by the delayed production of CO molecules beyond nanosecond time scales. [22] Given that such ongoing research continues to discover the process by which the parent molecules decompose, it is plausible that there may be slower rates of decomposition which may produce lower temperature and density environments of the reaction zone that could in turn facilitate the 'survival' of intact RDX crystals within the plasticiser matrix. These heated areas (which would reach the 478 K melting point of RDX) would cause initial deformation, including the folded and curled shapes of the observed particles.

Unlike the post-blast AlAN results, no spheroidal PE4 particles were found at 1 m from the detonations. The internal structures of post-blast PE4 also varied to that of AlAN found at 1 m, which were hollow (c.f. Figure 5e), and furthermore were different to that of the pre-blasted PE4 form, which were predominantly dense within (Figure 8a).

Instead, post-blast PE4 particles appeared internally as an arrangement of vertically aligned columns or rods, each being 120 nm to 170 nm in diameter (e.g. Figure 8d and e) (higher magnification images are provided in section 3 of the SI, Figure S-5 and S-6). These columns were not thought to be artefacts due to sample damage from the FIB procedure, however, the reason for their occurrence is unknown.

Figure 6. SEM micrographs of pre-blast particles: a) RDX crystals, b and c) PE4 particles. Representative post-blast particles observed on stubs positioned: 1 m from 0.5 kg PE4 detonations (d–g); at 2 m and 3 m (h–k); and at 4 m and 5 m (l–o).

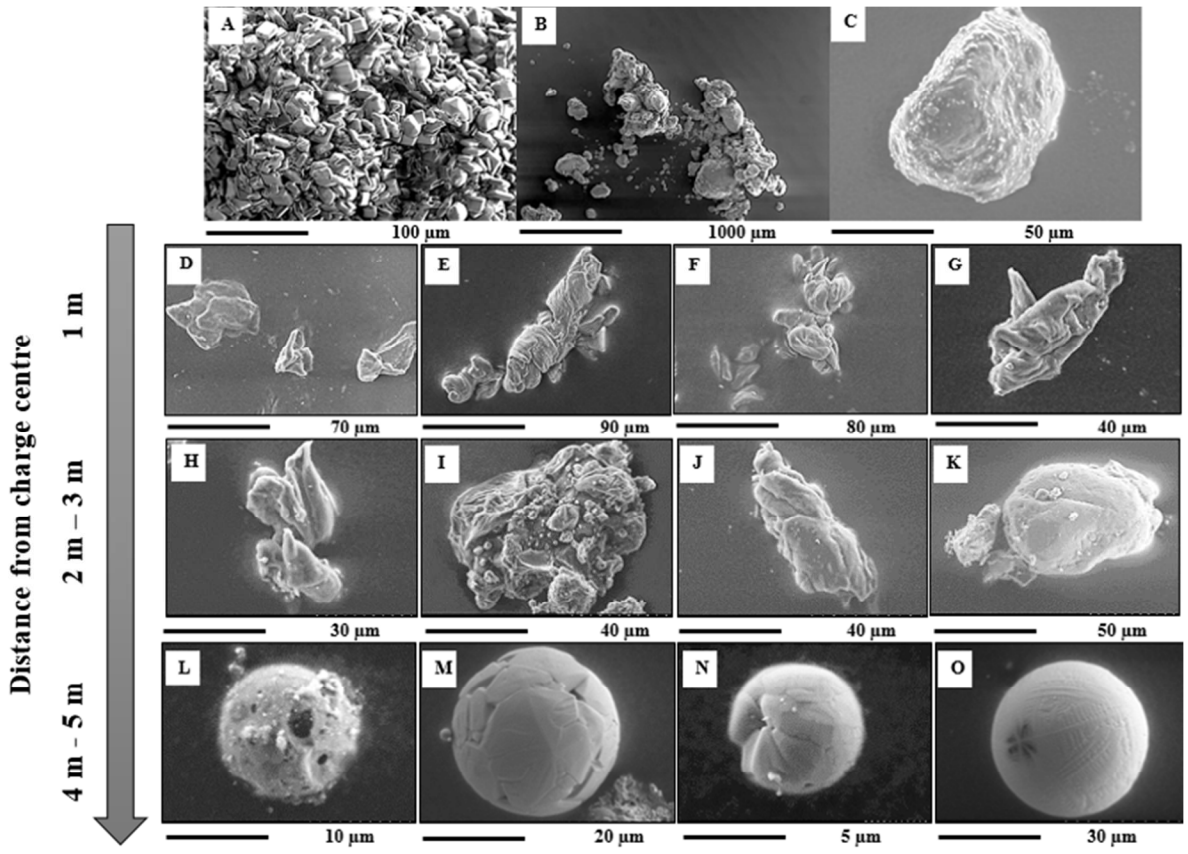

Figure 7. MeV SIMS spectrum (negative mode) of PE4 particles; pre-blast spectrum (red) compared to representative post-blast particle spectrum (black) and background (carbon disc) spectrum (green).

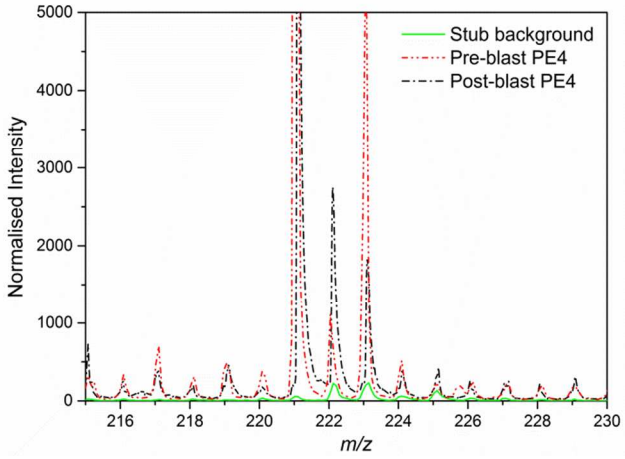

Further from the PE4 detonations, at 2 m and 3 m distances, the shapes of post-blast particles were consistent with those found at 1 m, but they were larger in size (63 % were 20 µm and 160 µm in diameter) (Figure 6h–k). After FIB-SEM analysis, the striations visible inside some of these particles' otherwise dense internal structure (Figure 8g and h) were considered artefacts of ion beam damage during milling. As the internal profiles of these post-blast particles were similarly solid to those of the pre-blast PE4 form (c.f. Figure 8a and b), it is plausible that PE4 residue may also have spalled from the bulk charge surface, as theorised for the AlAN explosive, yet retained less of the original particle morphology potentially due to the greater influence of heating effects.

Figure 8. SEM micrographs of the internal morphology of undetonated PE4 particles (a and b). Representative post-blast PE4 particles found at 1 m, prior to being milled (c), post-milling with the FIB (d, and close-up in e), and at 2 m - 3 m, prior to milling (f) and post-milling (g, and close-up in h).

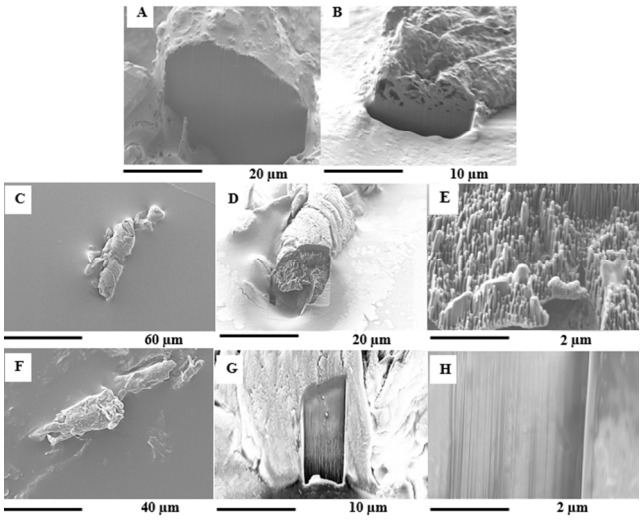

At distances of 4 m and 5 m, only very few, smaller spherical particles (56 % of which were 5 µm to 40 µm in diameter) were present (see Figure 6l–o). Whilst it was not possible to mill the particles found at these distances, no evidence from the internal or external morphology of particles found within a 3 m radius from the detonations suggested that they were formed upon cooling and condensation of vaporised matter, however these smaller spherical particles at 4 m and 5 m may indicate this occurring at further distances from the detonations of PE4. The greater energy release from the military composition may have caused the molten material to be projected further from the detonations (to 5 m) than was the case during the improvise AlAN charge firings (to 1 m). The sizes of these spherical residue particles found (5 µm to 40 µm) were consistent with previous findings regarding post-blast RDX. [10] While it has been possible here to use these findings to suggest mechanisms by which undetonated explosive material may remain following a complete detonation, further work is required to confirm the nature by which this occurs.

Qualitatively, particle-size counting showed that both fewer and smaller post-blast PE4 particles were observed compared to those of the inorganic formulation found at corresponding distances from the detonations (see Figure S-10 and section 4 of SI). In order to quantify the residue deposited onto each surface, filtered extracts from the stubs were analysed for RDX with HPLC-MS (average amounts were based on data from six firings of PE4). The total amount of RDX detected at each distance (the sum of four sampling sites) decreased with increasing distance from the detonation (102 ± 47 µg (1 m), 49 ± 24 µg (2 m), 11 ± 6 µg (3 m); see Figure S-11), similarly to that recorded for RDX in previous studies. [20,21] Though particles ascribed to be post-blast PE4 were observed up to 5 m from the detonation centres using SEM, reliable quantification of RDX was not achieved on samples retrieved further than 3 m away. This was potentially due to interferences from adhesive contaminants at lower explosive concentrations, which may have also caused an overall effect of lowering the amounts of RDX detected from all surfaces (further information and discussion on quantification issues is provided in section 4 of the SI). Overall however, the semi-quantitative trend observed with SEM corresponded well to the quantified amounts of deposited explosive residue.

No published literature to date has reported the particle size ranges and characteristic morphological differences of post-blast explosive residue reported herein. The majority of explosive particles were found to be larger than post-blast pyrotechnic residues identified from previous studies. [6 – 9] Clearly, distinctions between materials are likely and further energetic materials, in various confinements, should also be tested in order to assess the extent of variation between the appearances of their post-blast residues. The implications of these findings for forensic investigations are considerable, particularly if microscopic examination of material would be able to provide rapid initial explosive identification at a post-blast bomb scene. Additionally, the findings imply that the mechanisms by which explosive material may remain undecomposed in the first instance can vary depending on the material, which can now be probed further in order to develop our fundamental understanding of detonation.

Conclusion

By coupling traditional explosive residue analysis techniques with the original application of focused ion beam analysis to milling explosive particles, it has been possible to show that

different explosives produce morphologically variant post-blast particles. The ability to discriminate between the explosive charges fired based solely on the remaining residues has invaluable potential at post-blast crime scenes where the rapid nature of investigations requires fast results. The empirical evidence derived herein forms the beginnings of an evidence base concerning the behaviour of post-blast residues. Such an evidence base provides an essential first step for enabling forensically relevant interpretations of particulates in crime reconstructions; the importance of which for offering robust, reliable intelligence and evidence pertaining to the type of explosive used in terrorism cases is highly significant.

Understanding trace explosive particle morphology, density, and distribution, is also useful from an environmental perspective; knowledge on such factors would supplement remediation efforts applied to heavily used firing ranges that are used for training purposes. Further to applied scenarios, the findings also impact on our fundamental understanding of detonation phenomena by indicating that the mechanism by which the residues of each explosive type remain undetonated in the first place are different. It appears that AlAN is ejected from the bulk charge surface in a spallation-like effect, perhaps as molten material, whereas the PE4 may start to melt in lower–temperature regions during detonation, whilst both cool into the post-blast form principally during flight through the surrounding air.

Finally, as demonstrated herein, the complexity associated with post-blast explosive analysis necessitates not only the development of existing standard analysis techniques, but the application of more unconventional methods in order to probe further into discoveries about the nature of these materials.

ASSOCIATED CONTENT

Supporting Information. Additional information, as noted in text, is presented as a PDF file, available free of charge on the ACS Publications website. SI contains supplementary elemental and chromatographic analyses and quantification data and discussion.

AUTHOR INFORMATION

Corresponding Author

* nadia.abdul-karim.10@ucl.ac.uk

Author Contributions

All authors have given approval to the final version of the manuscript.

ACKNOWLEDGMENT

N.A-K acknowledges funding received from the UK Engineering and Physical Sciences Research Council (EPSRC Grant code: EP/G037264/1). Jim Clements, Graeme Creighton and Paul Walker are thanked for their help on the Explosive Range Demonstration Area, Cranfield University. Two anonymous reviewers are thanked for their helpful comments and advice for this manuscript.

REFERENCES

[1] R. Strobel, in Forensic Investigation of Explosions, (Ed: A. Beveridge), Taylor and Francis Ltd., Salisbury, UK 1998 Ch. 5.

[2] S. Zitrin, J. Yinon, Modern Methods and Applications in Analysis of Explosives, Wiley and Sons, Ltd. Chichester, UK. 1996.

[3] N. Abdul-Karim, C. S. Blackman, P. P. Gill, E. M. M. Wingstedt, B. A. P. Reif, RSC Adv. 2014, 4, 54354.

[4] J. D. Kelleher, Forensic Sci. Comms. 2002, 4.

[5] S. L. Lancaster, M. Marshall, J.C. Oxley, in Wiley Encyclopaedia of Forensic Science, (Eds: A. Jamieson, A. Moenssens), Wiley and Sons, Ltd., New York, USA 2009

[6] E. Vermeij, W. Duvalois, R. Webb, M. Koeberg, Forensic Sci. Int 2009, 186, 68.

[7] K. L. Kosanke, R.C. Dujay, B. J. Kosanke, J Forensic Sci. 2003, 48, 531.

[8] K. L. Kosanke, R.C. Dujay, B. J. Kosanke, J Forensic Sci. 2006, 51, 296.

[9] S. A. Phillips, Science and Justice 2001, 41, 73.

[10] S. Taylor, E. Campbell, L. Perovich, J. Lever, J. Pennington, Chemosphere 2006, 65, 1405.

[11] D. Pantea, S. Brochu, S. Thiboutot, G. Ampleman, G. Scholz, Chemosphere 2006, 65, 821.

[12] M. Kotrlý , I. Turková, in Proc. SPIE CBRNE Sensing XV, Vol 9073, Maryland, USA, 2014.

[13] S. Burgess, X. Li, J. Holland, Microscopy and Analysis 2013, 27, S8.

[14] D. J. Wedlock, Controlled Particle, Droplet and Bubble Formation, Butterworth-Heinemann Ltd., Jordan Hill, Oxford, UK. 1994 Ch. 6.

[15] D. Cranney, R. Bingham, L. Mckenzie, (Dyno Nobel, Inc) US 20140216616 A1, 2014.

[16] E. I. V van den Hengel, R. J. A. Kersten, F. A. M. H. Jacobs, R. Oostdam, N. H. A. Versloot, in IChemE Sympos. Series, No. 153, Edinburgh, UK, 2007.

[17] P. Kommisarov, B. S. Ermolaev, B. A. Khasainov, H. N. Presles, in Proc. 34th Int. Pyrotech. Seminar, Beaune, France, 2007, 8.

[18] B. S. Ermolaev, A. A. Sulimov, V. E. Khrapovskii, V. A. Foteenkov, Russ. J. Phys. Chem. B. 2011, 5, 640.

[19] P. Kolla, A. Sprunkle, J Forensic Sci. 1995, 40, 406.

[20] J. C. Pennington, T. F. Jenkins, G. Ampleman, S. Thiboutot, J. M. Brannon, A. D. Hewitt, J. Lewis, S. Brochu, E. Diaz, M. R. Walsh, M. E. Walsh, S. Taylor, J. C. Lynch, J. Clausen, T. A. Ranney, T. A. Ramsey, C. A. Hayes, C. L. Grant, C. M. Collins, S. R. Bigl, S. Yost, K. Dontsova, Distribution and Fate of Energetics on DoD Test and Training Ranges: Final Report, Engineer Research and Development Centre, 2006.

[21] N. Abdul-Karim, R. Morgan, R. Binions, T. Temple, K. Harrison, J Forensic Sci. 2013, 58, 365.

[22] I. V. Schweigert, J. Phys. Chem. A 2015, 119, 2747.

FOR TOC ONLY

Authors are required to submit a graphic entry for the Table of Contents (TOC) that, in conjunction with the manuscript title, should give the reader a representative idea of one of the following: A key structure, reaction, equation, concept, or theorem, etc., that is discussed in the manuscript. Consult the journal's Instructions for Authors for TOC graphic specifications.

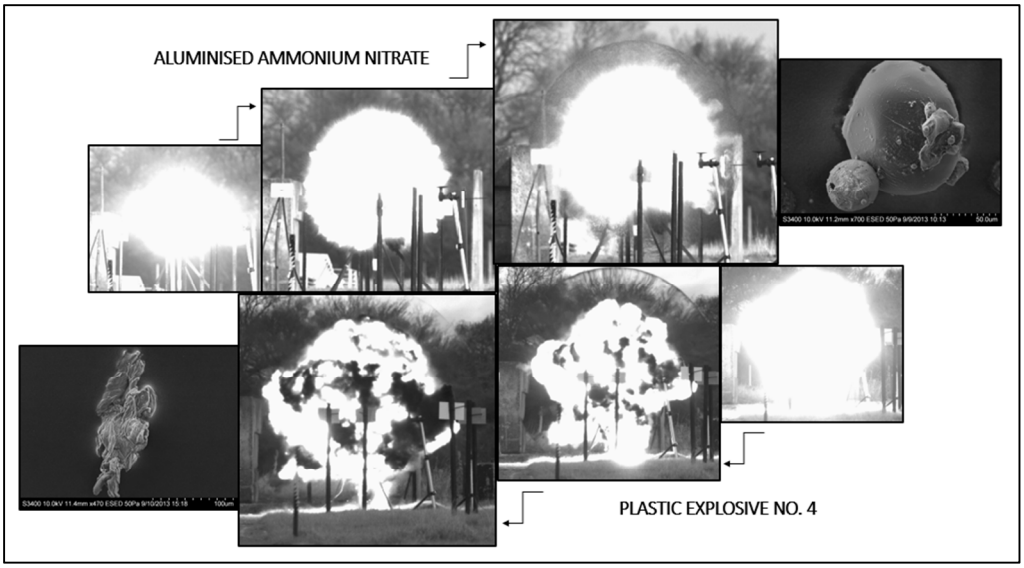
ALUMINISED AMMONIUM NITRATE
PLASTIC EXPLOSIVE NO. 4

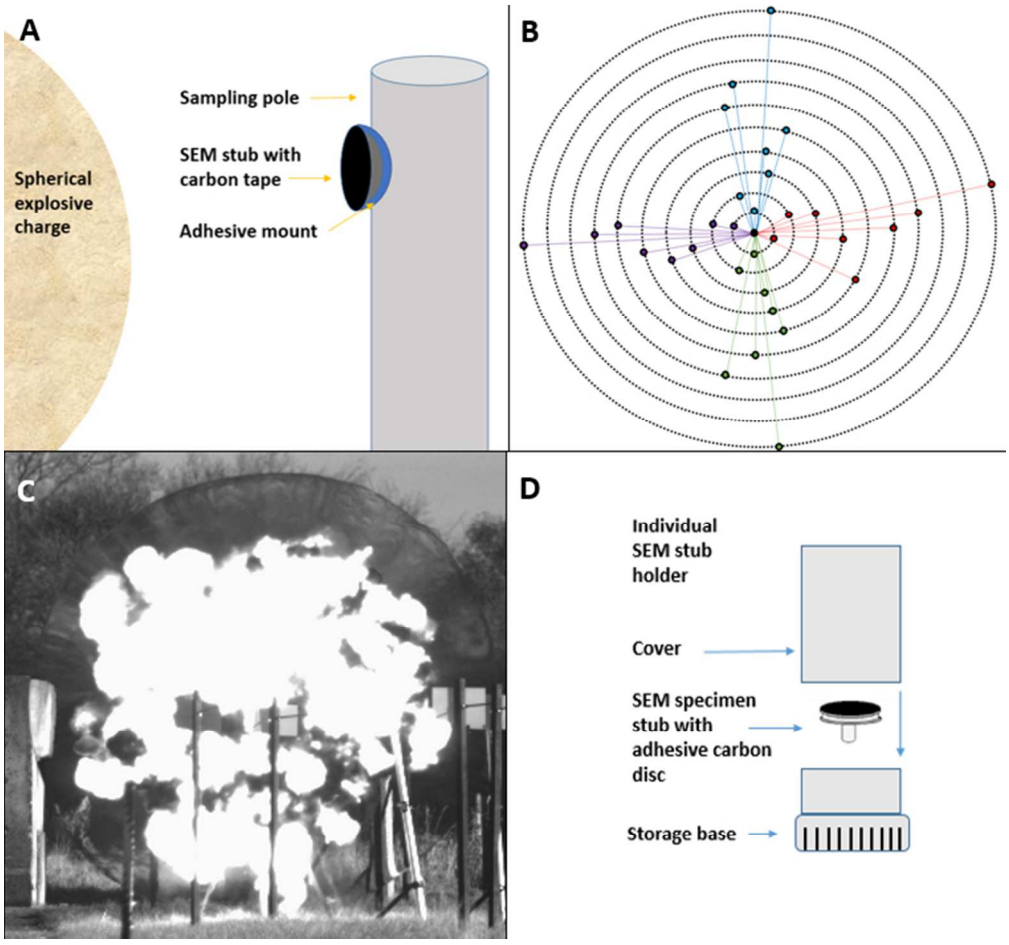

Figure 1. Schematics of sampling pole layout and stub arrangement around detonations: a) placement of SEM stubs onto steel sampling poles using adhesive mounts, b) aerial view of the sampling poles (black) positioned at 1 m incremental distances around the central explosive charge, c) example of fireball during detonation of PE4 charge, and d) individual sample holders used to store collected stubs following each firing.
200x186mm (96 x 96 DPI)

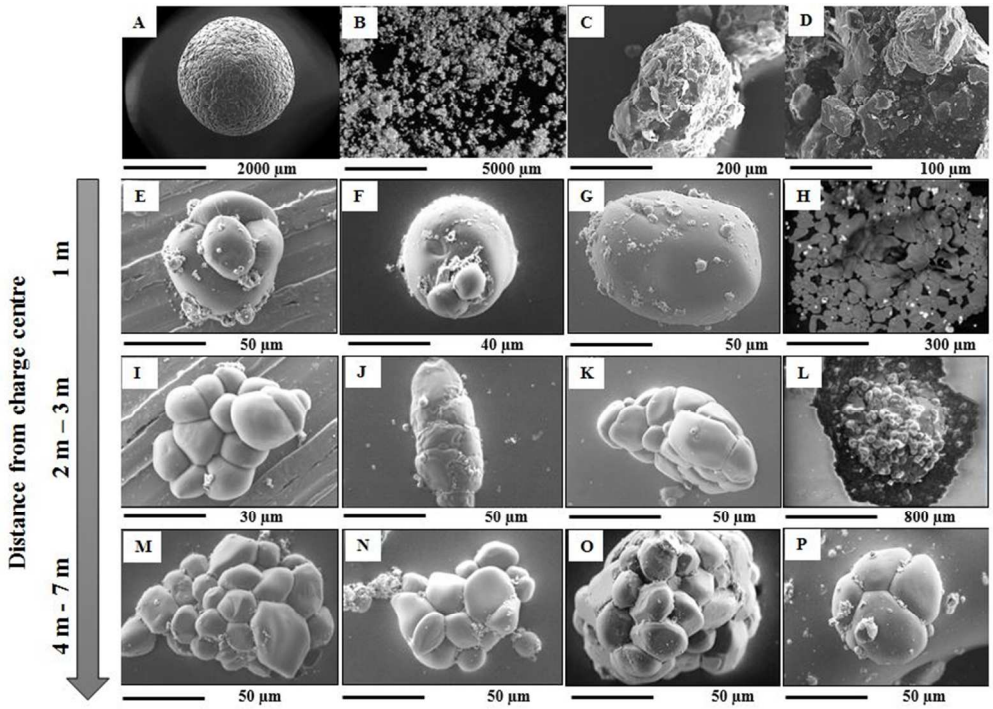

Figure 2. SEM micrographs of a) AN prill surface, b) ground AN particles, c) AN particles once mixed with Al, d) close-up of Al flakes on AN particle surface, e–h) representative post-blast particles observed on stubs retrieved 1 m from the detonations of 0.5 kg AlAN charges, i–l) particles retrieved from 2 m and 3 m distances, m–p) particles retrieved from 4 m to 7 m distances.
231x164mm (96 x 96 DPI)

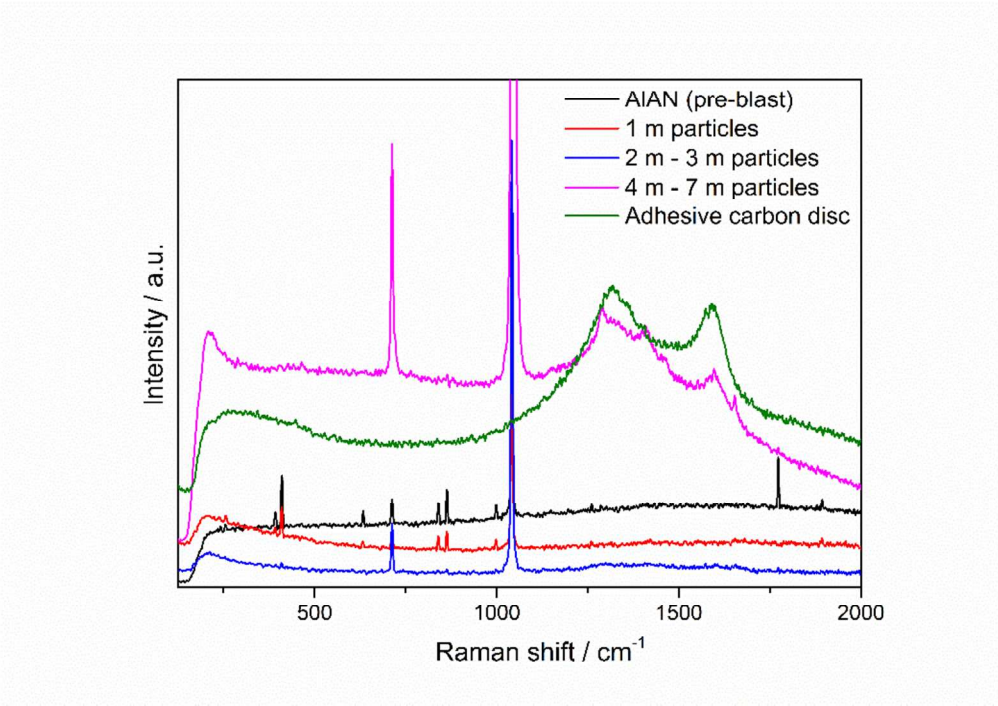

Figure 3. Raman spectrum of pre-blast AlAN particles (black) compared to representative spectra of post-blast particles collected at 1 m (red), 2 m to 3 m (blue), and 4 m to 7 m (pink) from the detonations. The green spectrum is of the adhesive carbon background.
120x85mm (220 x 220 DPI)

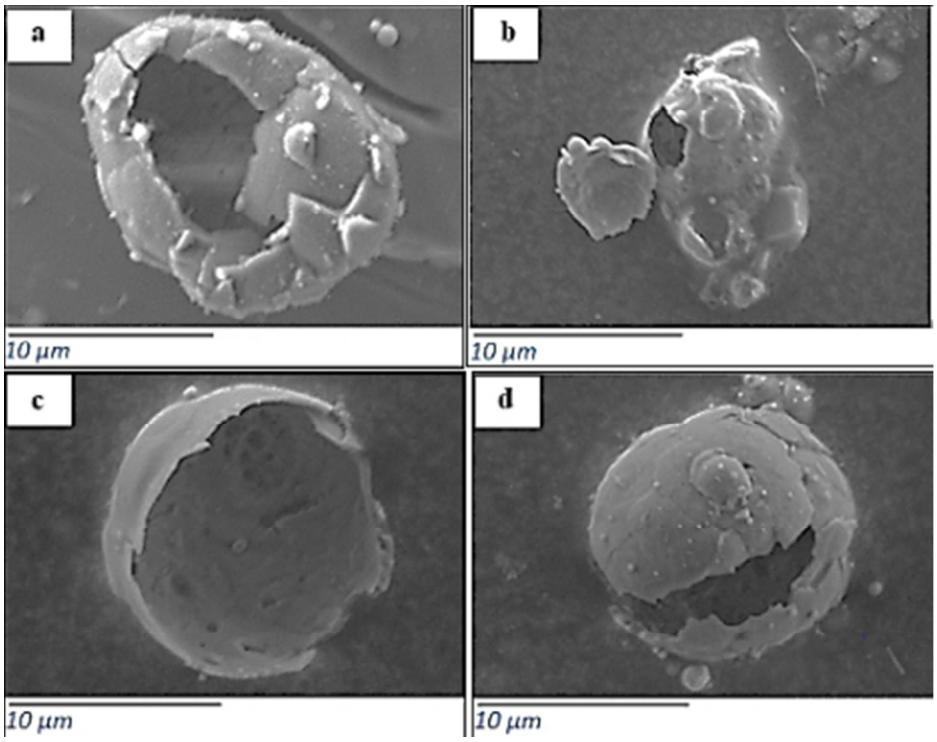

Figure 4. Hollow particles and particle clusters observed on stub surfaces that were positioned 1 m from the detonations of 0.5 kg AlAN charges.
53x42mm (220 x 220 DPI)

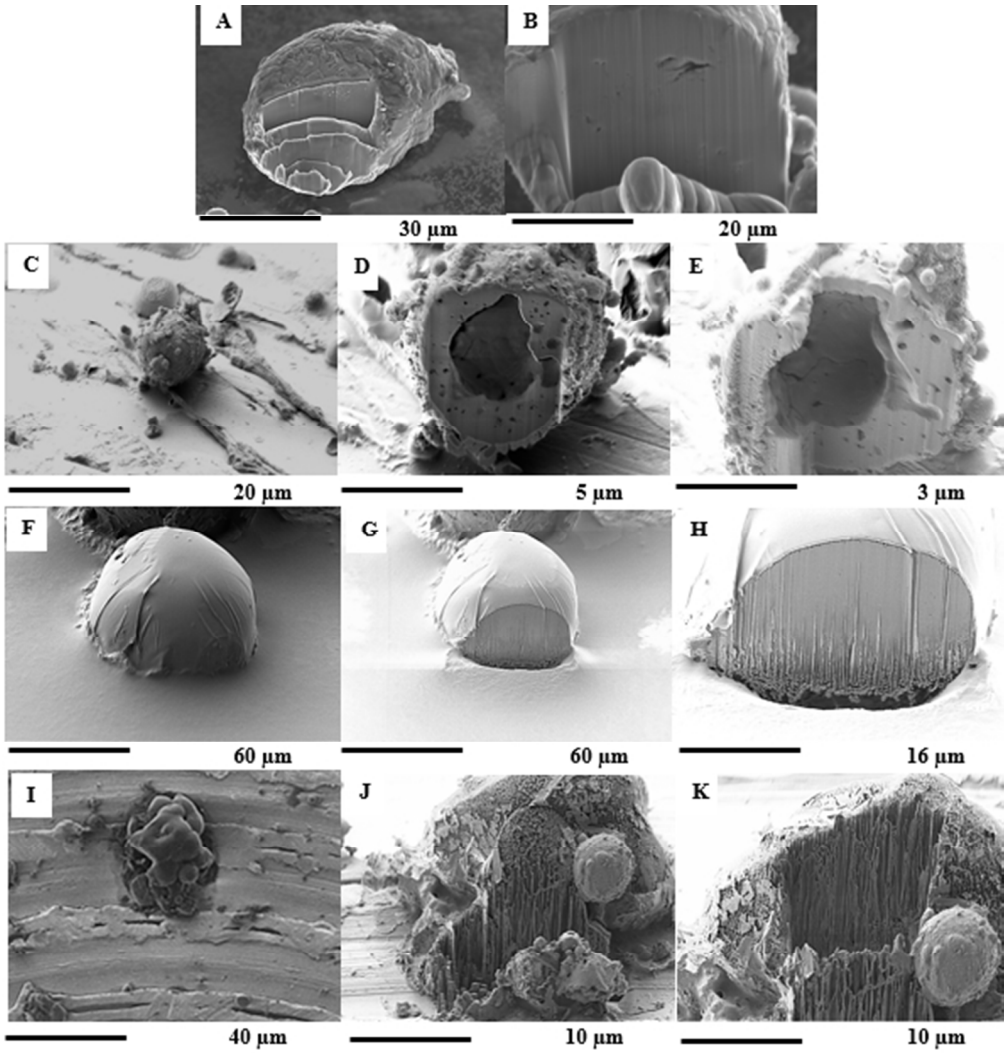

Figure 5. SEM micrographs of the internal morphology of undetonated AlAN particles (a and b). Micrographs of post-blast particles prior to being cut (c, f, i), after milling (d, g, j), and close-ups of the internal structure (e, h, k) for: spherical particles with surface features found at 1 m from detonations (c - e); smooth surfaced spheroidal particles from 2 m away (f - h); and aggregated particle clusters found 5 m away (i - k). 156x164mm (96 x 96 DPI)

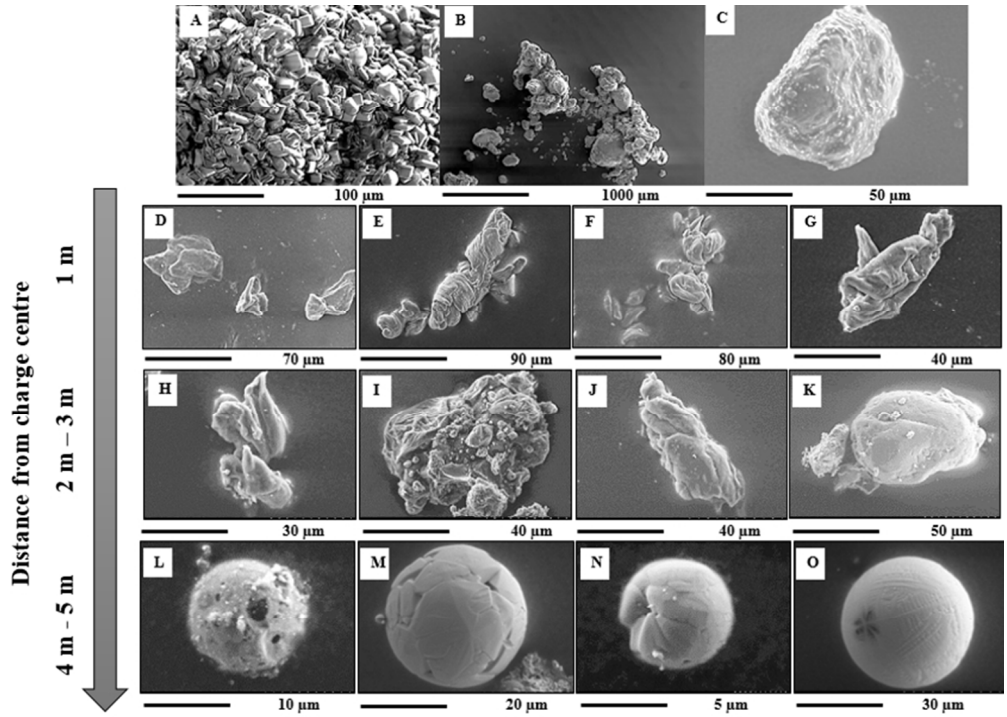

Figure 6. SEM micrographs of pre-blast particles: a) RDX crystals, b and c) PE4 particles. Representative post-blast particles observed on stubs positioned: 1 m from 0.5 kg PE4 detonations (d–g); at 2 m and 3 m (h–k); and at 4 m and 5 m (l–o).
222x159mm (96 x 96 DPI)

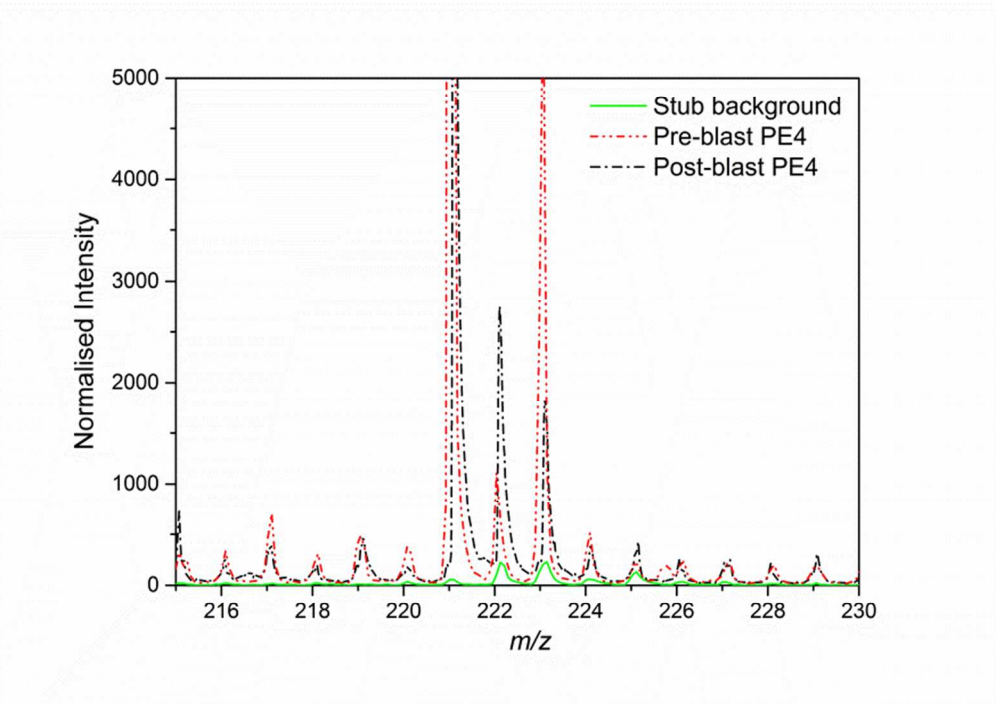

Figure 7. MeV SIMS spectrum (negative mode) of PE4 particles; pre-blast spectrum (red) compared to representative post-blast particle spectrum (black) and background (carbon disc) spectrum (green).
232x164mm (96 x 96 DPI)

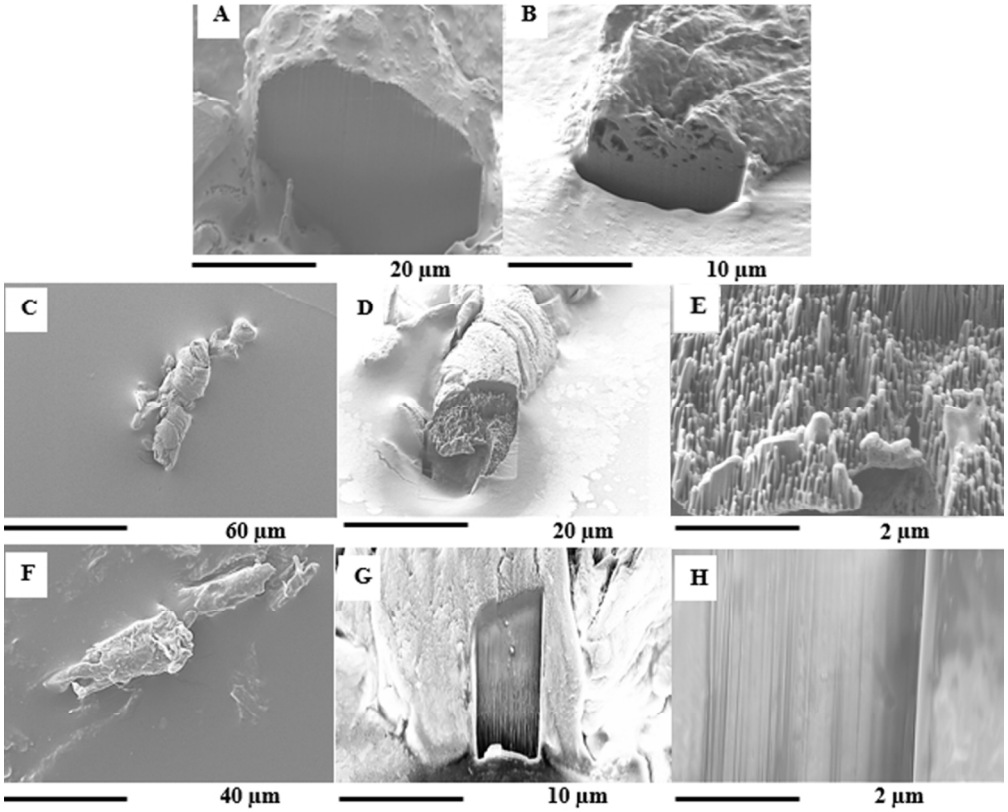

Figure 8. SEM micrographs of the internal morphology of undetonated PE4 particles (a and b). Representative post-blast PE4 particles found at 1 m, prior to being milled (c), post-milling with the FIB (d, and close-up in e), and at 2 m - 3 m, prior to milling (f) and post-milling (g, and close-up in h).
232x188mm (96 x 96 DPI)